physica p s s status solidi

reprints

WILEY-VCH

REPRINT

physica status solidi

www.pss-b.com

basic solid state physics
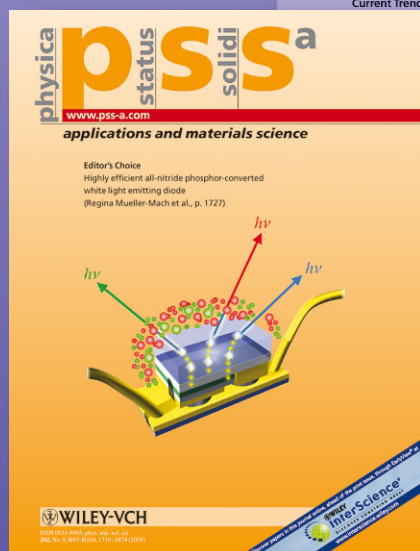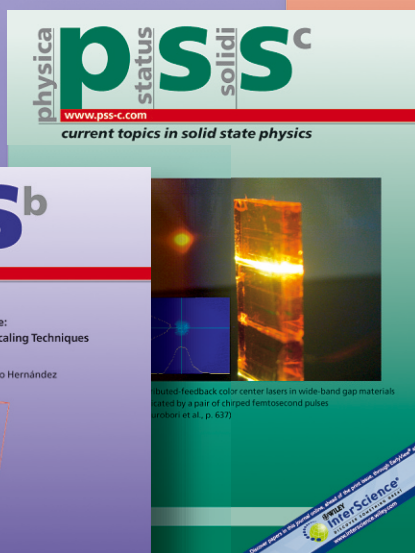
Hydrogen and carbon interaction in a FeNi alloy with a vacancy

Estela Gonzalez[1], Paula Jasen[1], Gabriel Gonzalez[2], Lilian Moro[1, 2], and Alfredo Juan[*, 1]

[1] Departamento de Física, Universidad Nacional del Sur, Av. Alem 1253, 8000 Bahía Blanca, Argentina
[2] Departamento de Ingeniería Mecánica, Facultad Regional Bahía Blanca, Universidad Tecnológica Nacional, 11 de abril N° 461, 8000 Bahía Blanca, Argentina

[*] Corresponding author: e-mail cajuan@uns.edu.ar, Phone: +54 291 459 5142, Fax: +54 291 459 5142

The bonding of hydrogen and carbon to Fe and Ni in a 50:50 alloy is analysed using density functional calculations. The changes in the electronic structure of a $L1_0$ alloy upon C and H introduction at a vacancy region are addressed and a comparison with H or C in pure metals is drawn. H in bulk FeNi alloy with a vacancy locates at a tetrahedral site shifted towards the vacancy. Instead, C prefers an octahedral site (Fe based). The vacancy acts as strong traps of both C and H. Fe–Ni atoms are initially more strongly bonded to each other due to the vacancy formation. Consequently, the Fe–Fe, Fe–Ni and Ni–Ni bond strengths are diminished as new metal–C or metal–H bonds are formed. The most affected bond is the Fe–Ni, whose overlap population decreases by 72%. An analysis of the orbital interaction reveals that the Fe–H bonding involves mainly the Fe 4s, H 1s and Ni 4s orbitals. In the case of the sequential absorption, the C–H interaction is almost zero at a distance of 2.72 Å. The main interactions of these interstitials are developed with either Fe or Ni. We also consider the absorption sequence (H first or C first) and its influence on the electronic structure. Our results could be relevant to understand some steps of the carburization process during thermal cracking operations where hydrogen atoms are present.

1 Introduction FeNi alloys are used in aircraft engines, steam turbines in power generation plants and in medical, nuclear, chemical and petrochemical industries. Their more important properties are their low expansion, electrical resistance, shape memory and soft magnetization.

The ambient-pressure temperature composition structural phase diagram of FeNi is complicated and is still being elaborated [1, 2]. It includes a Fe-rich body-centred-cubic (BCC) phase (α-phase), a face-centred-cubic (FCC) phase (γ-phase) that can be metastably quenched over a broad composition range 0–70 at% Fe at room temperature; INVAR and ELENVAR are two such alloys; a low-spin FCC phase (γ_{LS}-phase) and chemically ordered FCC phases centred at ~50 and ~25 at% Fe (FeNi and FeNi₃ phases, respectively). Also, a chemically ordered Fe₃Ni FCC phase has been proposed but its existence has never been substantiated by experimental evidence. In addition, high pressures stabilize a nonmagnetic hexagonal close-packed (HCP) phase (ε-phase) [3–5] that is closely related to the γ_{LS}-phase [2].

There are few ab initio theoretical calculations in the open literature on the properties of Fe–Ni clusters. Kaspar and Salahub have earlier used the self-consistent-field Xα scatter-wave method to explain, from a molecular point of view, several of the INVAR anomalies [6]. The study of the equilibrium geometries also enabled Rao et al. to see if there is any tendency of Fe and Ni to segregate, i.e., if Fe–Ni bonding is less favoured over Fe–Fe and Ni–Ni bonding [7]. Guenzburger and Ellis computed the electronic structure of the ordered phase of FeNi [8].

The electronic properties and magnetic behaviour of FeNi alloys have been of special interest since 1897 when Guillaume first reported an almost zero thermal expansion over a wide temperature range in FCC crystals with Ni concentration of around 35 at% [9]. This behaviour was subsequently observed in various ordered and random bi-

nary alloy systems, and became known as the "INVAR effect" [10].

Interest in understanding the physics of hydrogen in metals and alloys has been continuously increasing for many reasons. On one hand, there are practical uses of metal−hydrogen systems such as storage of hydrogen for clean energy purposes, catalysts and absorption of nuclear radiation; on the other hand, there are unwanted effects on the material properties caused by small amounts of hydrogen dissolved in metals, such as embrittlement, crack propagation and corrosion. There is extensive literature dealing with these issues, ranging from first-principles calculations to engineering applications [11−20].

Carbon is one of the most important alloying elements in Fe. In addition to the useful effect of carbides in the mechanical properties of steels, with only small additions it has a decisive effect on the deformation behaviour and many other properties of steel. Many of the effects of carbon on steel properties originate from strong interactions between interstitial carbon atoms and various defects such as vacancies, self-interstitials, dislocations and grain boundaries [21]. The aging and temperature behaviour of iron−Ni−carbon and iron−carbon martensite have been reported by van Genderen et al. [22].

Recently, the electronic structure and the features of chemical bonding in Fe crystal containing carbon impurities were discussed in detail [23−27]. In particular, the question of the charge transfer in the Fe−C bond is of great interest.

Jiang and Carter studied the location of C in the bulk in BCC iron and the adsorption and diffusion into Fe(110) and Fe(100) by density functional theory (DFT) [28, 29]. Their prediction of O site preference for C on bulk and on the subsurface of Fe(100) agrees with the experiments.

Widely present in materials, vacancies have strong interactions with other defects such as impurities. These interactions greatly affect the mechanical properties of the material. To understand the role of C it is important to characterize its interaction with defects at the atomic level.

Domain et al. have reported the study of foreign C atoms interacting with vacancy point defects in α-Fe. These authors found a strong binding energy of C with vacancies by DFT calculations [30]. Using positron-lifetime measurements, Hautojärvi et al. have concluded that during vacancy migration at 220 K an asymmetric vacancy−carbon pair is formed [31].

In a previous work, our group has reported that the addition of a C atom in a Fe BCC matrix that contains a vacancy decreases the strength of the local Fe−Fe bond to about 78% of its original value. This bond weakening is a consequence of a C−Fe bond formed at the expense of the Fe−Fe neighbour bonding [32].

The aim of the present paper is to find the location of C and H in a FeNi model alloy and to understand the effect of the impurities on the electronic structure.

2 Computational method Gradient-corrected density functional theory (GC-DFT) calculations were performed on a supercell containing 88 atomic sites in a $L1_0$ lattice to model bulk FeNi, with a $4 \times 4 \times 4$ reciprocal space grid in the supercell Brillouin zone (BZ) and a plane-wave kinetic energy cutoff of 220 eV for the Fe−Ni−H−C system [33−35].

We used a periodic density functional theory (ADF-BAND) [36]. The molecular orbitals were represented as linear combinations of Slater functions. The Becke [37] gradient correction approximation for the exchange energy functional and the B3LYP [38] approximation for the correlation functional were employed. In order to increase the computational efficiency, the innermost atomic shells of electrons are kept frozen for every atom except hydrogen or carbon, since the internal electrons do not contribute significantly to the bonding.

We have used a triple-zeta basis set (this means three Slater-type functions for each atomic valence orbital occupied) with polarization functions to express the atomic orbitals of Fe and Ni. The basis set of Fe consisted of 3d, 4s and 4p orbitals and 3d and 4s for Ni. With this set we obtained a magnetic moment of $2.26\mu_B$ for BCC Fe, which compares very well with the experimental value of $2.20\mu_B$ [39]. The accurate quadratic tetrahedron procedure [40] was used for Brillouin zone integrations, and integration parameters were chosen to achieve convergence within 50 meV.

The geometry was optimized until the changes in the energy gradient and in the Cartesian coordinates were 0.001 Hartree/Å and 0.01 Å, respectively. Only the Fe or Ni atoms' first neighbours to the vacancy were allowed to relax. After finding the most stable position for the impurities in the zone near the vacancy, we studied the Fe−H−C and the Ni−H−C interactions.

To understand the Fe−Ni−H−C interactions we used the concepts of density of states (DOS) and overlap population density of states (OPDOS). The DOS curve is a plot of the number of orbitals as a function of the energy. The integral of the DOS curve over an energy interval gives the number of one-electron states in that interval; the integral up to the Fermi level (E_F) gives the total number of occupied molecular orbitals. If the DOS is weighed with the overlap population between two atoms the overlap population density of states OPDOS is obtained. The integration of the OPDOS curve up to E_F gives the total overlap population of the specified bond orbital and it is a measure of the bond strength [41]. If an orbital at a certain energy is strongly bonding between two atoms the overlap population is strongly positive and the OPDOS curve will be large and positive around that energy. Similarly, a negative OPDOS around a certain energy corresponds to antibonding interactions [42]. It should be mentioned that another method to measure the bond strength has been recently published [43].

The absorption energy was computed as the difference ΔE between the Fe−Ni−H and the Fe−Ni−C composite

systems when the C or the H atom is absorbed in its minimum energy geometry and when it is far away from the Fe−Ni alloy. It can be expressed as

$$\Delta E_{total} = E(Fe_{m-1}Ni_m + X) - E(Fe_{m-1}Ni_m) - E(X) ,$$

where E is the total energy, m indicates the number of atoms in the cell and $E(X)$ is the energy of the impurity (C, H or both) in vacuum.

We have considered the interaction of C and H simultaneously in the Fe−Ni matrix. We have also tested the absorption sequence starting with C or H.

3 Model of the FeNi alloy with a vacancy We have studied C and H absorption in the $L1_0$ FeNi phase alloy structure using a supercell of 87 + V (vacancy) atoms, distributed in seven layers of the (001) plane. The FeNi phase (CuAu(I)) has a lattice parameter $a = 3.592$ Å [44]. We found a value of 3.589 Å for the lattice parameter. The crystal structure is shown in Fig. 1a.

We notice that the FeNi structure no longer has cubic symmetry but is, in fact, tetragonal ($L1_0$). In this work, it

was modelled as having cubic structure because the distortion is small [44, 45].

The structure has three types of interstitial sites, one tetrahedral (T) and two octahedral. All T are equivalent with the same chemical environment around the site (see Fig. 1b). The two octahedral sites are O1 based on Ni and O2 based on Fe atoms (see Fig. 1b).

To study the absorption of C or H we mapped the energy surfaces with 0.01 Å steps in the central region of the cluster with cuts perpendicular to the (001) planes (see Fig. 1c and d). After determining the more stable position for the first impurity atom, we have studied the electronic interaction between these interstitials and the metallic atoms.

4 Results and discussion
4.1 FeNi alloy Let us discuss first the electronic structure of the FeNi perfect alloy and the FeNi alloy with a vacancy in absence of the impurities. Table 1 summarizes the results for the electron occupation, variation of charge and overlap population (OP) for both systems. In the perfect
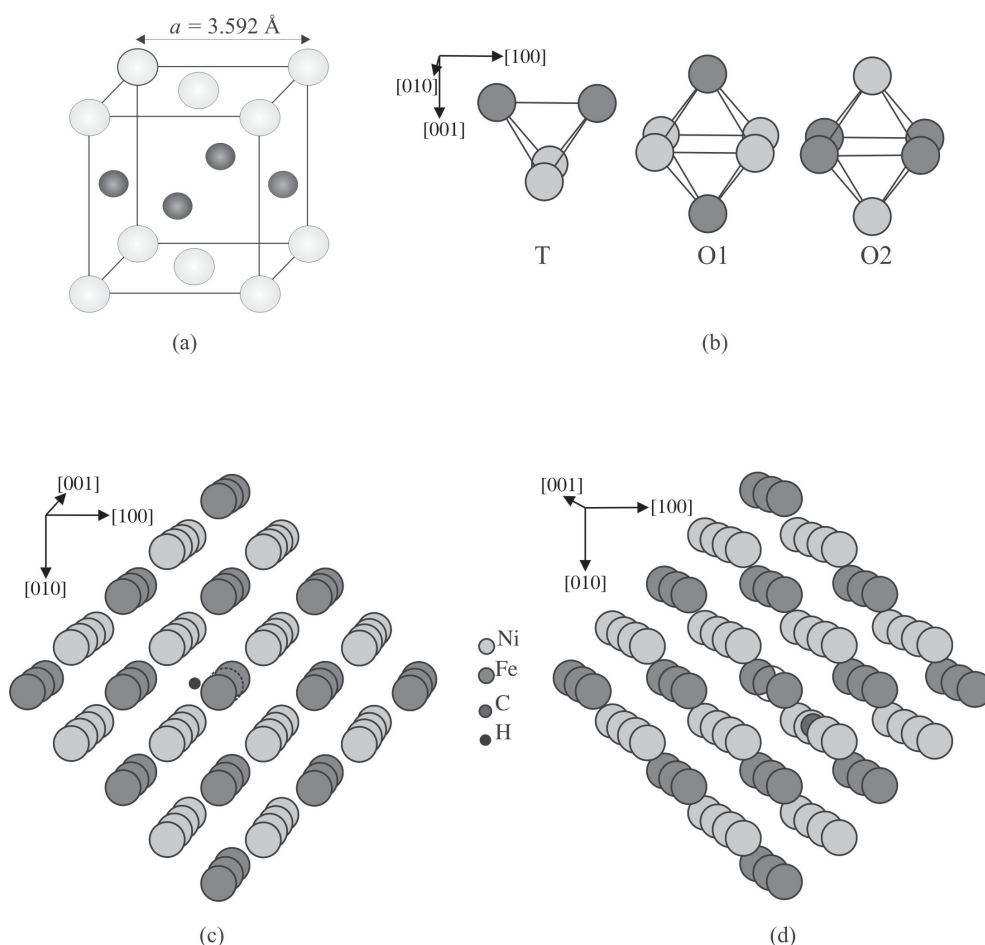

Figure 1 Schematic view of the unit cell of FeNi alloy (a). Schematic representation of the three interstitial sites of the alloy: tetrahedral (T), octahedral based on Ni (O1) and octahedral based on Fe (O2) (b). Schematic view of the FeNi + V alloy cluster after the H (c) or C (d) absorption.

Table 1 Electron occupation, overlap population (OP), charges and distances for the FeNi perfect alloy and with a Fe vacancy.

structure	electron occupation			Δ charge[*]	bond type	OP	ΔOP (%)	distance (Å)
	s	p	d					
FeNi								
Fe	0.51	0.06	4.30		Fe−Fe	0.222		2.53
Ni	0.86	0.94	9.37		Ni−Ni	0.281		
					Fe−Ni	0.168		
FeNi−V								
Fe	0.51	0.08	4.34	−2.02	Fe−Fe	0.225	+1.35	
Ni	0.87	0.94	9.42	+5.39	Ni−Ni	0.306	+8.9	
					Fe−Ni	0.194	+15.5	

[*] The percentages of change in electronic charge and OP are computed with respect to the perfect alloy.

alloy case, the OP for the metal−metal bond is similar to that corresponding to the pure metals (0.210 for BCC Fe or 0.148 for FCC Ni). The introduction of the vacancy reorganizes the charge, increasing the density mainly on the Fe atoms. All the metal−metal OPs are increased. Whereas the levels near the Fermi level (E_F) are antibonding in the pure solid, now the metals present lower coordination caused by the loss of a metallic atom. Thus, the system acquires a higher stability due to a decrease in the population of antibonding states. The most favourable OP change occurs for the intermetallic bond (15.5%). The DOS curves for FeNi with a Fe vacancy (see Fig. 2) show similarities with that obtained for the pure alloy. The major Ni contribution corresponds to the region of (−15, −10) eV, whereas the Fe contribution is mainly up to −11 eV with a small contribution at lower energies.

The OPDOS curves for the pair near to the vacancy are shown in Fig. 3. The Fe−Fe bond near to the E_F level is antibonding to be later bonding. The Ni−Ni bond is almost totally bonding. The antibonding interaction is moderated with the vacancy introduction.

4.2 H absorption H is eccentrically located to the vacancy with a distance of 1.16 Å from its centre and near a T site (0.41 Å from it). It is 0.67 eV more stable than the same location in the perfect alloy (see Fig. 1c). The Ni−H distance is lower than the Fe−H distance (see Table 2). These results are similar to the preliminary ones calculated by Anderson [46]. In the case of H/Fe(110), Moritz et al. determined by Low Electron Energy Diffration (LEED) a Fe−H distance of 1.75 Å [47]. Recently, Ashman et al. reported that the Ni−H bond lengths do increase with cluster size and coverage from 1.47 Å in Ni−H to 1.64 Å in Ni_4H_2 [48]. The H atom is charged negatively, as was previously reported by our group and others [13].

Figure 4 shows the DOS curves after the H absorption. The only visible difference is the appearance of an H-based state at −16.3 eV. It can be observed that the Fe−H interaction is more developed that the Ni−H one.
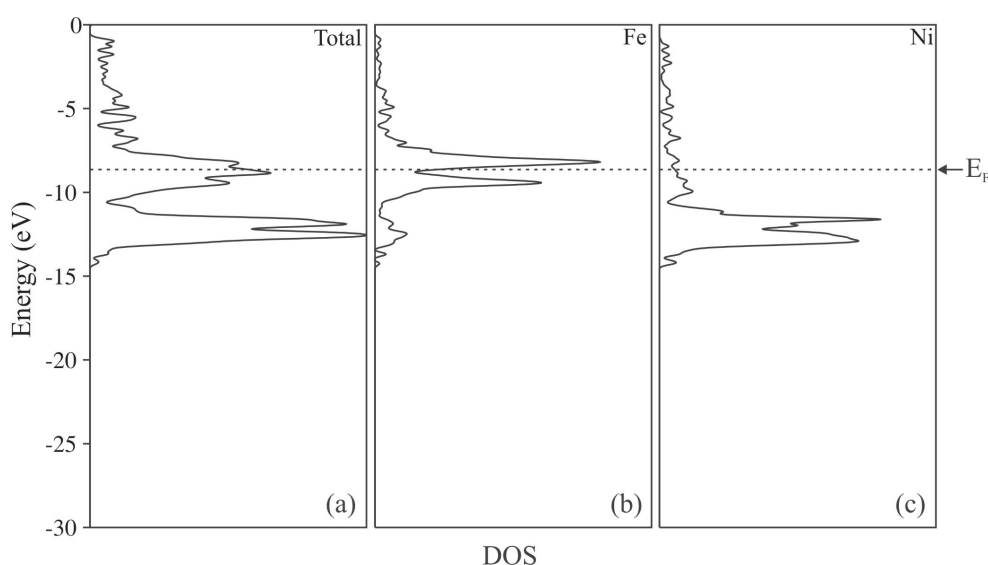

Figure 2 DOS curves for the FeNi alloy with a vacancy. Total (a), projected on a Fe atom (b) and on a Ni atom (c). The scale in (b) and (c) is 100×.
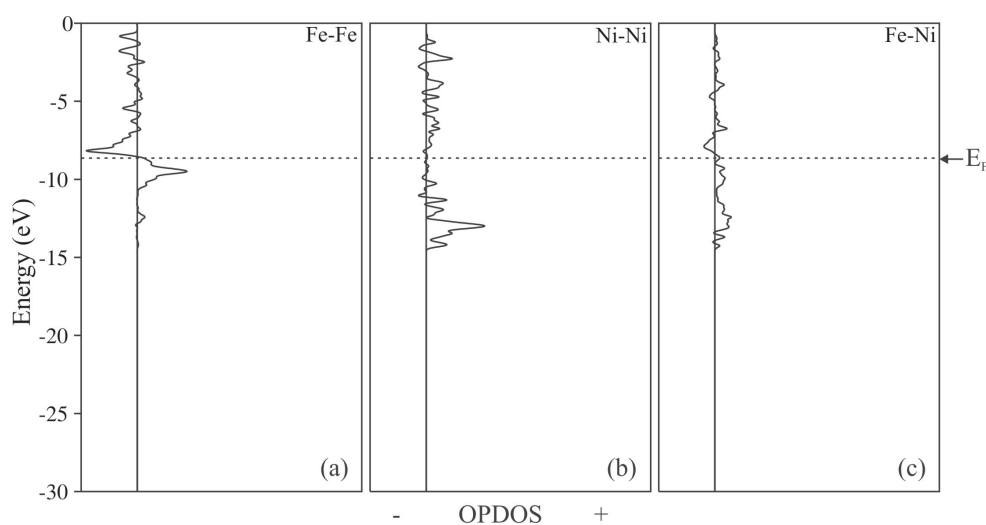
Figure 3 OPDOS curves for the FeNi alloy with a vacancy. Fe–Fe (a), Ni–Ni (b) and Fe–Ni (c) bonding.

Table 2 Electron occupation, overlap population (OP), electronic charges and distances for the Fe–Ni–H–C composite system[*].

| absorption sequence	electron occupation			charge	bond type	OP	distance (Å)
	s	p	d				
(FeNi–V) + H							
Fe$_I$	0.46	0.04	4.29	3.210	Fe$_I$–Fe$_{II}$	0.222	2.533
					Fe$_{III}$–Fe$_{IV}$	0.225	
Ni$_I$	0.86	0.91	9.43	−1.197	Ni$_I$–Ni$_{II}$	0.257	2.533
Fe$_{III}$	0.44	0.04	4.14	3.377	Fe$_{III}$–Ni$_I$	0.195	2.533
H	1.22	0.00	0.00	−0.225	Ni$_{III}$–H	0.382	1.645
Ni$_{III}$	0.77	0.94	9.42	−1.230	Fe$_I$–H	0.126	1.849
(FeNi–V) + C							
Fe$_{IV}$	0.46	0.16	4.96	2.410	Fe$_{IV}$–Fe$_V$	0.114	2.533
Ni$_I$	0.77	0.96	9.24	−1.196	Ni$_I$–Ni$_{II}$	0.240	2.533
Fe$_{III}$	0.44	0.05	4.14	3.377	Fe$_{III}$–Ni$_I$	0.053	2.533
C	1.35	3.60	0.00	−0.957	Fe$_{III}$–C	0.506	1.801
					Ni$_I$–C	0.649	1.801
(FeNi–V) + C + H							
Fe$_{IV}$	0.47	0.05	4.31	3.169	Fe$_{IV}$–Fe$_V$	0.114	2.533
Ni$_I$	0.77	0.96	9.24	−0.976	Ni$_I$–Ni$_{II}$	0.241	2.533
Fe$_{III}$	0.44	0.04	4.14	3.377	Fe$_{III}$–Ni$_I$	0.054	2.533
C	1.35	3.60	0.00	−0.956	Ni$_I$–C	0.650	1.801
					Fe$_{III}$–C	0.511	1.801
H	1.25	0.00	0.00	−0.254	Fe$_I$–H	0.103	1.967
Ni$_{IV}$	0.77	0.96	9.35	−1.112	Ni$_{IV}$–H	0.488	1.560
					C–H	0.001	2.717
(FeNi–V) + H + C							
Fe$_I$	0.46	0.05	4.30	3.192	Fe$_I$–Fe$_{II}$	0.223	2.533
					Fe$_{III}$–Fe$_{IV}$	0.105	
Ni$_I$	0.76	0.94	9.25	−0.949	Ni$_I$–Ni$_{II}$	0.207	2.533
Fe$_{III}$	0.44	0.04	4.16	3.358	Fe$_{III}$–Ni$_I$	0.057	2.533
H	1.22	0.00	0.00	−0.218	Ni$_{III}$–H	0.400	1.645
Ni$_{III}$	0.78	0.95	9.36	−1.082	Fe$_I$–H	0.139	1.849
					Fe$_{IV}$–C	0.389	1.908
C	1.35	3.59	0.00	−0.940	Ni$_I$–C	0.648	1.795
Fe$_{IV}$	0.46	0.16	4.93	2.450	H–C	0.004	2.506

[*] The geometry is shown in Fig. 6.
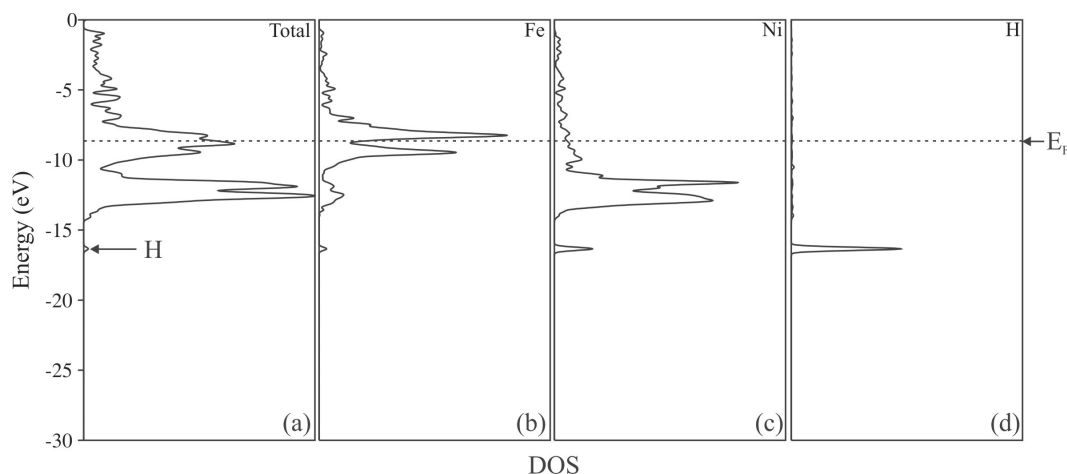
Figure 4 DOS curves for the FeNi + V alloy after H absorption. Total (a), projected on a Fe atom (b), on a Ni atom (c) and on an H atom (d). The scale in (b)–(d) is 100×.

Regarding the chemical bonding, the Ni–Ni and the Fe–Ni OPs diminish by 50%. A decohesion effect had been previously reported in pure solids [11]. The Ni–H OP is greater than the Fe–H one. That situation is predictable from the fact that H forms reversible hydrides with Ni while for Fe they only occur at several GPa [49]. This effect can be observed in the OPDOS curves shown in Fig. 5.

4.3 C absorption The most favourable site for C location in a perfect FeNi lattice is the O1 hole. Experiments show that interstitial C stays mainly in the octahedral sites of the FCC Fe lattice [50]. An embedded atom method calculation for C in the FCC Fe–C system also predicts the octahedral site preference while the dilute heat of solution of carbon is calculated to be 0.3 eV [21]. In our case, the solution enthalpies for C in the relaxed cell indicate a slightly exothermic process of about 0.33 eV. For the sake of comparison, we also calculated the solution enthalpy of C in the T site for the FeNi perfect structure and we found that it is about 45% less favourable than the O1 site. In the case of the O2 site, the difference is about 9% in favour to the O1 site.

When the C atom is absorbed in the FeNi alloy in the region near the vacancy, the more stable geometry locates the impurity close to an O2 site (0.18 Å from it), which is 0.15 eV more stable than the same location in the perfect alloy (see Fig. 1d). Whereas C absorption is a much more favourable process than H absorption in the FeNi alloy, the absorption energy difference between the perfect alloy and the alloy with the vacancy is much lower. Such a situation can be understood by the tendency of C to form stable iron or nickel carbides, while a stable iron hydride is only formed at several GPa [49].
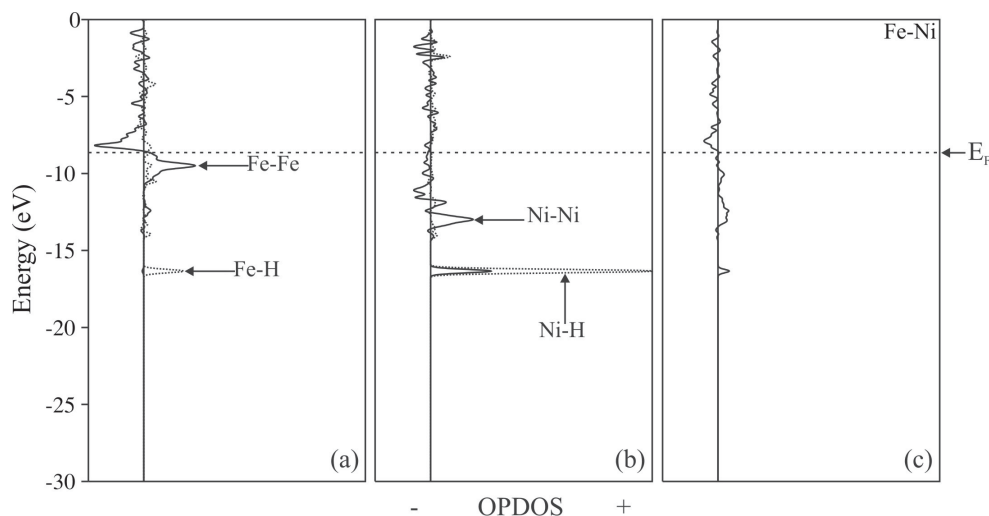

Figure 5 OPDOS curves for the FeNi + V alloy after H absorption. Fe–Fe and Fe–H (a), Ni–Ni and Ni–H (b) and Fe–Ni (c) bonding.

Original
Paper

Phys. Status Solidi B **246**, No. 6 (2009)   1281
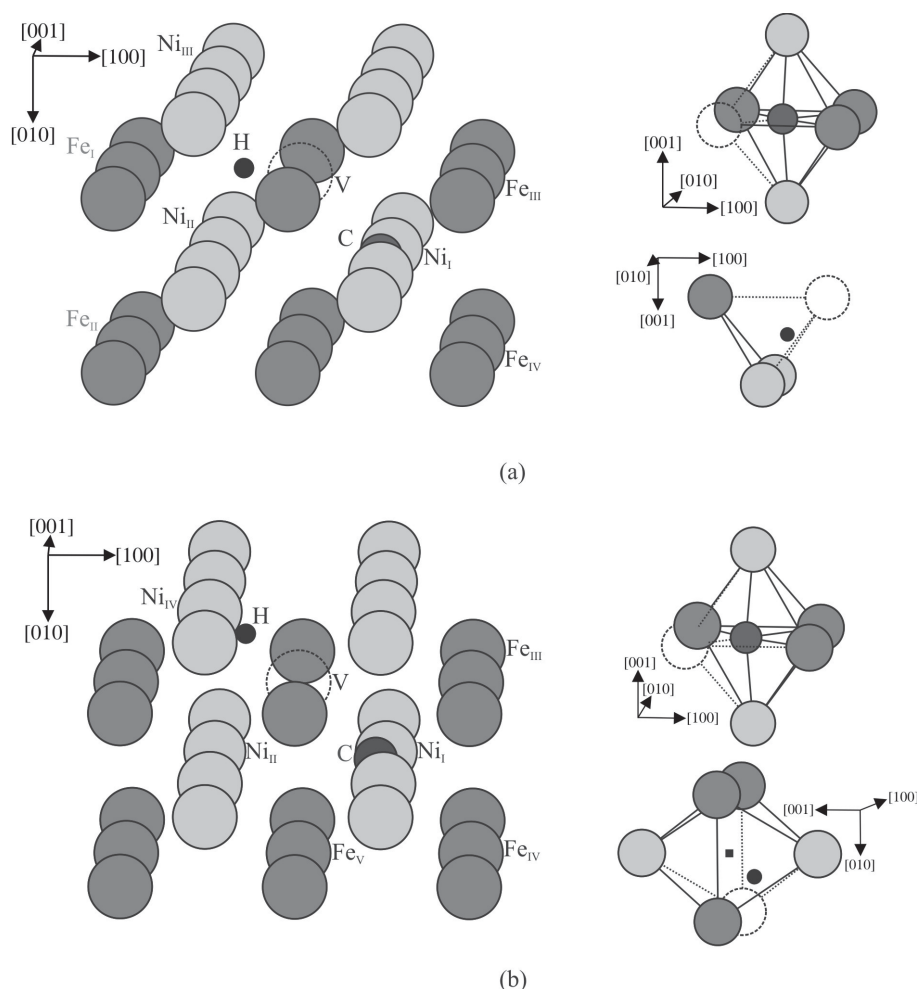
Figure 6 Schematic view of the frame absorption H−C (a) and C−H (b) in the FeNi + V alloy. The left-hand plots show the absorption site for each impurity. The black square indicates the center of the octahedral site.

The C atom is located at 1.60 Å from the centre of the vacancy and at 1.80 Å from both metals. In a recent work, Tzeli and Mavridis reported that in gas phase diatomic species Fe−C and Ni−C present bond distances from 1.5 Å to 2.0 Å [51]. The Fe−C distance is similar to that reported by Niu et al. near a dislocation core in α-Fe of 1.84 Å [52] and by Wu et al. on the (111) surface (1.80 Å) [53]. Fournier et al. reported a Ni−C distance of 1.77 Å on a Ni(100) surface [54]. Experimental determinations by Onuferko et al. [55] and Bader et al. [56] found a C−Ni(100) distance of 1.80−1.82 Å. The measured value for the first-neighbour Fe−C distance in Fe−Ni C austenite is 1.886 Å [57]. Carbon is found to prefer off-centre sites from the vacancy and maintains a distance of 1.77 Å from nearest Fe atoms [58]. Our computed C-vacancy binding energy is 37 kJ/mol, in good agreement with experimental measurements and theoretical calculations of Slane et al. in Fe−35% Ni alloy [59].

Table 2 shows that C generates a strong interaction with both Fe and Ni. The Fe−Fe and Fe−Ni bonds are weakened with a reduction in their OPs of up to 72%, the intermetallic bond being the most affected. The impurity C is negatively charged as is predictable, receiving the main

transference from the neighbouring Fe of $-0.957e^-$. A similar charge transfer was reported for interstitial C located at octahedral sites in Fe clusters [60].

The electronic charge on C in FCC iron based alloy has been a matter of debate since the electromigration experiments of Seith [61] and Nakajima and Hirano [62]. DFT calculations of Press et al. [58] determined an ionicity on C in $Fe_{14}C$ + vacancy from -0.23 to -0.50. Morinaga et al. [26, 27] determined an ionicity on C in FCC Fe of -0.347. Krause et al. [63] computed an acceptor character of C in FCC Fe observing an inflow of electrons of $-0.37e^-$ towards the impurity. On the other hand, Gavriljuk et al. found that C enhances localization of electrons at the iron atoms in γ-Fe containing up to 5% of C [64].

Figure 7 shows the DOS curves after the C absorption. Three regions can be observed in the C projection. The zone at -18 eV corresponds to the C 2s based states and the zones at -15 eV and -12 eV correspond to the C 2p based states.

For the Fe−C bond, most of the bonding states are filled while the antibonding states are pushed upward above the Fe 3d band. The bonding states originate mainly via C 2s and 2p and Fe 4s and 4p with a small contribution
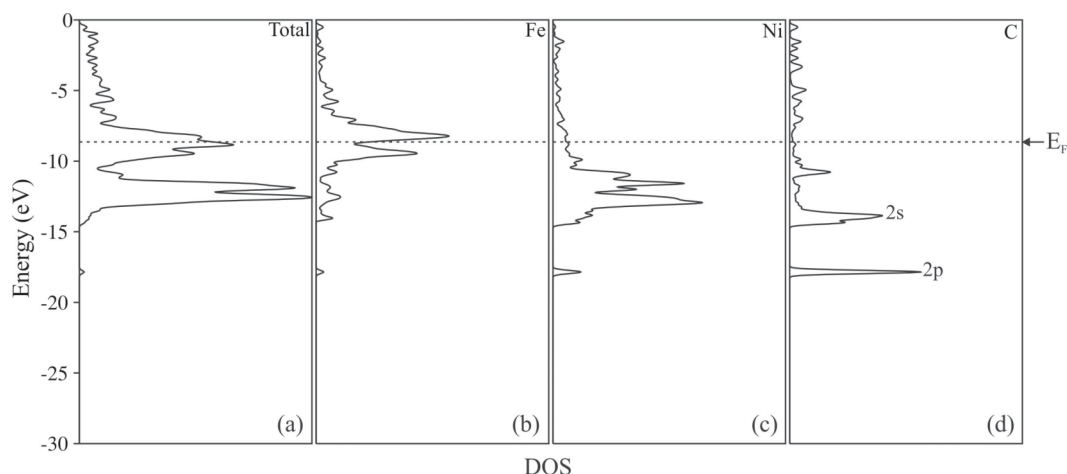
Figure 7 DOS curves for the FeNi + V alloy after C absorption. Total (a), projected on a Fe atom (b), on a Ni atom (c) and on a C atom (d). The scale in (b)−(d) is 100×.

of 3d orbitals. In particular, the two peaks observed in the curves of Figs. 7 and 8 indicate strong bonding interaction between C and Fe. The lowest energy, at −17.9 eV, is mainly C 2s−Fe 4s interaction while the one at −13.7 eV is composed mostly of C 2p and Fe 4p states. The overlap population for the Fe−C interaction for the Fe neighbours to C is 0.506. The C does not affect the bonding strength between Fe second neighbours. Regarding the chemical bonding, the OPDOS curves in Fig. 8 show that the Fe−C interaction is always bonding, while the Ni−C interaction is bonding up to −11.6 eV and then becomes antibonding.

Calculated results for C, N and O interstitial atoms in FCC Fe have been given by Morinaga et al. [26] using the self-consistent discrete variational Xα cluster method. These authors have shown the existence of strong metal−metalloid bonds, which are primarily due to Fe 3d−C (or −N) 2p covalent interactions [27]. According to the

charge density distribution, the Fe−C covalent bonding comes from the weak p−d σ-type interaction. Also, the bond strength was found to be strongly dependent on the displacements of the iron atoms near an interstitial atom [65].

4.4 H absorption with C pre-absorbed With a C atom residing in its minimum position, we moved the H atom along the vacancy region and then optimized the new geometry. The minimum Fe−H and Ni−H distances proved to be 1.967 Å and 1.560 Å. The final location for the H atom is eccentrically to an O2 site (0.81 Å from its centre) and towards the vacancy (1.15 Å), as shown in Fig. 6b. Recently, Petkov et al. have computed the Ni−H and Ni−C distances. Using an ab initio methodology, these authors reported 1.66 Å and 1.81−1.84 Å, respectively [66].
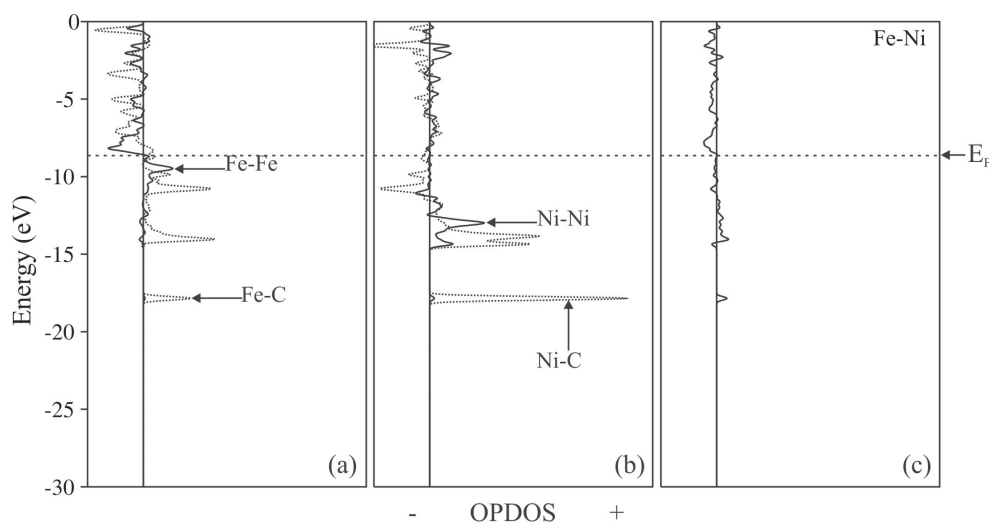

Figure 8 OPDOS curves for the FeNi + V alloy after C absorption. Fe−Fe and Fe−C (a), Ni−Ni and Ni−C (b) and Fe−Ni (c) bonding.

Original

Paper

Phys. Status Solidi B **246**, No. 6 (2009)   1283
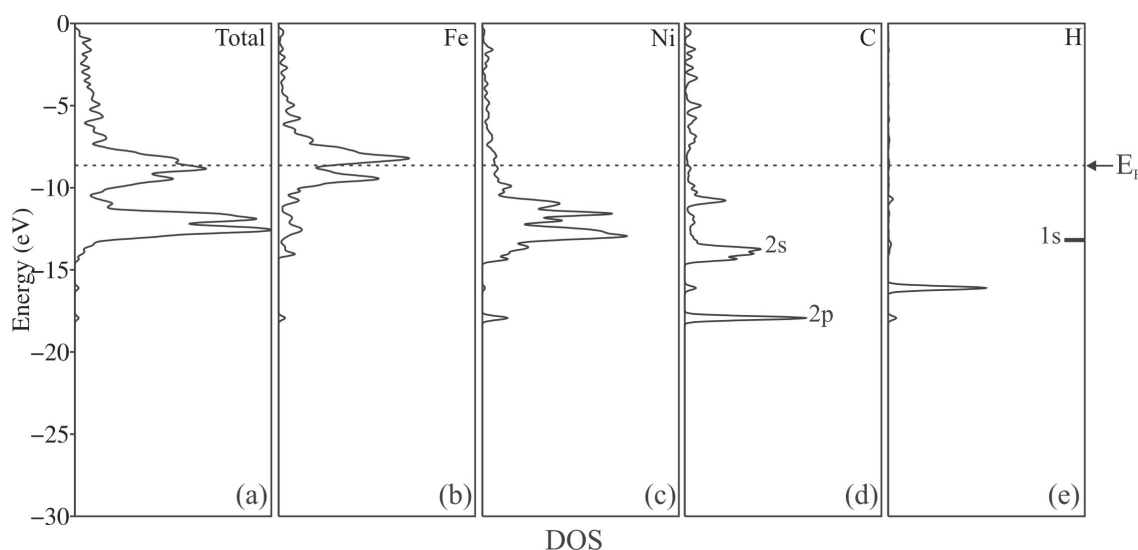
Figure 9 DOS curves for the FeNi + V + C alloy after H absorption. Total (a), projected on a Fe atom (b), on a Ni atom (c), on a C atom (d) and on an H atom (e). The scale in (b)−(e) is 100×.

The changes in the OP, in Table 2, are computed as a difference from the system with a C or an H (in that case, C would be the second introduced impurity). It can be seen there that the changes in the OP are much lower after H introduction, if we compare the values with respect to the system with C pre-absorbed. The C−H interaction is very weak at a distance of 2.717 Å. A similar distance has been reported in [67]. As a reference, the C−H bonding distance in saturated hydrocarbons is about 1.10 Å [68].

H does not accumulate in the neighbourhood of the C. The experimental information indicates that C acts as expeller of H and prevents the weakening of the Fe−Fe bond at the dislocation core. Another important aspect related to grain boundary strength is the beneficial effect of carbon.

It has been reported that 185 ppm carbon can prevent the intergranular fracture due to hydrogen [69].

When H is located in the C-containing system, it does not practically affect the DOS plot (compare Figs. 7 and 9); it only presents a split-off state below the d band, which is located at 6.8 eV below E_F. In a recent publication, our group has reported that state to be 7.1 eV from E_F in the case of BCC Fe with a vacancy [70].

The total DOS curve for the cluster with C and H atoms (Fig. 9) looks almost similar to the cluster without impurities (Fig. 2). The differences are the peaks that emerge below the d metal band that correspond to C- and H-based states. The impurity-based peaks are centred at lower energy values, which represent an additional energetic stabi-
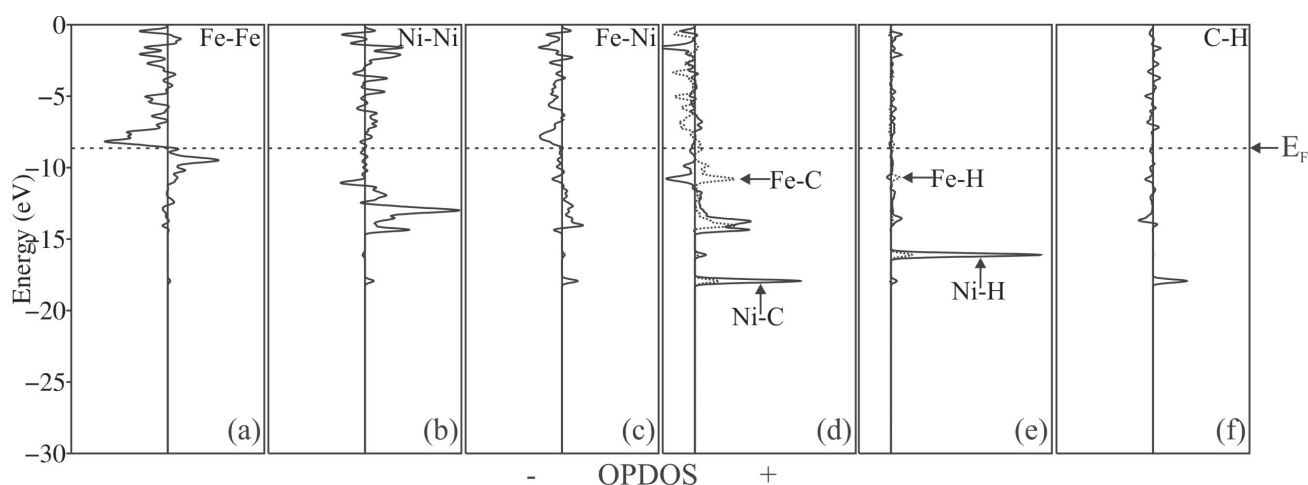

Figure 10 OPDOS curves for the FeNi + V + C alloy after H absorption. Fe−Fe (a), Ni−Ni (b), Fe−Ni (c), Fe−C and Ni−C (d), Fe−H and Ni−H (e) and C−H (f) bonding.

lization in the vicinity of the vacancy. The small contribution of the impurities to the DOS is due to their low concentration.

Regarding the bonding, the OPDOS curves are plotted in Fig. 10. The interaction is almost bonding except for Fe−Fe bonds in a region close to E_F. As mentioned in [39], H as an impurity debilitates the Fe−Fe bonds. The presence of C increases the Ni−H bond if we compare it with the case of H alone. As mentioned before, C also decreases the OP between nearest-neighbour Fe and Ni atoms. However, the spatial distribution of C orbitals makes it possible that sorts of Fe−C−Fe and Ni−C−Ni bridges could be established. The Fe−C−Fe OPs are 0.511 and 0.344, while the Ni−C−Ni OPs are 0.650 and 0.652. Such bridges could prevent the displacement of the metallic layers.

A change in the absorption sequence considering first the H and afterwards C presents similar results with only a slight energy difference (0.07 eV) in favour of this case. In both configurations C resides in similar positions, the H being moved according to the absorption sequence. Again, the C−H interaction is almost zero at a distance of 2.51 Å.

5 Conclusions The system is stable when C or H is absorbed, being more favourable in the first case. In the case of C absorption, the impurity is located in an octahedral O1 site, meanwhile the H is located at a tetrahedral site. Both impurities decrease the metal–metal bonding, but the H has an OP stronger than the Ni while the C has OPs with similar strengths with both metals. The decohesive effect of H is well known in pure metals and alloys, whereas the C effect is still debated. Certainly, the strength of the OP for the metal−metal bonding decreases but a metal−C−metal interplanar bonding formation is possible. The C−H interaction is almost null in both sequences of absorption. The final H−metal or C−metal distances are similar to that reported from theoretical calculations and experiments.

References

[1] K. B. Reuter, D. B. Williams, and J. I. Goldstein, Metall. Trans. A **20**, 719 (1988).

[2] D. G. Rancourt and R. B. Scorzelli, J. Magn. Magn. Mater. **150**, 30 (1995).

[3] T. Takahashi, W. A. Bassett, and H. K. Mao, J. Geophys. Res. **73**, 4717 (1968).

[4] E. Huang, W. A. Bassett, and M. S. Weathers, J. Geophys. Res. **93**, 7741 (1988).

[5] H. K. Mao, Y. Wu, L. C. Chen, J. F. Shu, and A. P. Jephcoat, J. Geophys. Res. **95**, 21737 (1990).

[6] J. Kaspar and D. Salahub, Phys. Rev. Lett. **47**, 54 (1981).

[7] B. K. Rao, S. Ramos de Debiaggi, and P. Jena, Phys. Rev. B **64**, 024418 (2001).

[8] D. Guenzburger and D. E. Ellis, Phys. Rev. B **36**, 6971 (1987).

[9] C. E. Guillaume, C. R. Acad. Sci. **125**, 235 (1897).

[10] E. F. Wassermann, in: Ferromagnetic Materials, edited by K. H. Buchow and E. P. Wohlfarth, Vol. 5 (Elsevier, Amsterdam, 1990), chap. 3, pp. 237−322.

[11] Y. Fukai, in: The Metal−Hydrogen System, edited by U. Gonser et al., Springer Series in Materials Science, Vol. 21 (Springer, Berlin, 1993), chap. 3, p. 55.

[12] M. Ruda, D. Farkas, and J. Abriata, Phys. Rev. B **54**, 9765 (1996).

[13] P. Nordlander, J. K. Nørskov, and F. Besenbacher, J. Phys. F, Met. Phys. **16**, 1161 (1986).

[14] P. Wiswall, in: Hydrogen in Metals II, edited by G. Alefeld and J. Völkl (Springer, Berlin, 1978), p. 201.

[15] T. Schober and H. Wenzl, in: Hydrogen in Metals II, edited by G. Alefeld and J. Völkl (Springer, Berlin, 1978), p. 11.

[16] H. Sugimoto and Y. Fukai, Phys. Rev. B **22**, 670 (1980).

[17] R. Griessen and A. Driessen, Phys. Rev. B **30**, 4372 (1984).

[18] P. Fiebelman and D. Hamann, Solid State Commun. **34**, 215 (1980).

[19] A. R. Williams, J. Kubler, and C. D. Gelatt, Phys. Rev. B **19**, 6094 (1979).

[20] C. D. Gelatt, H. Ehrenreich, and J. A. Weiss, Phys. Rev. B **17**, 1940 (1979).

[21] B. L. Lee, Acta Mater. **54**, 701 (2006).

[22] M. J. van Genderen, M. Isac, A. Böttger, and E. J. Mittemeijer, Metall. Mater. Trans. A **28**, 545 (1997).

[23] V. G. Gavriljuk, Distribution of Carbon in Steels (Naukova Dumka, Kiev, 1987).

[24] C. Demangeat, M. A. Khan, and J. C. Parlebas, J. Magn. Magn. Mater. **15–18**, 885 (1980).

[25] K. Lee, J. Callaway, K. Kwong, R. Tang, and A. Ziegler, Phys. Rev. B **31**, 1796 (1985).

[26] M. Morinaga, N. Yukawa, H. Adachi, and T. Mura, J. Phys. F, Met. Phys. **18**, 923 (1988).

[27] M. Morinaga, N. Yukawa, H. Adachi, and T. Mura, J. Phys. F, Met. Phys. **17**, 2147 (1988).

[28] D. Jiang and E. A. Carter, Phys. Rev. B **67**, 214103 (2003).

[29] D. Jiang and E. A. Carter, Phys. Rev. B **71**, 045402 (2005).

[30] C. Domain, C. Becquart, and J. Foct, Phys. Rev. B **69**, 144112 (2004).

[31] P. Hautojärvi, J. Johansson, A. Vehanen, J. Yli-Kauppila, and P. Moser, Phys. Rev. Lett. **44**, 1326 (1980).

[32] S. Simonetti, E. Pronsato, G. Brizuela, and A. Juan, Phys. Status Solidi B **244**, 610 (2007).

[33] P. Hohenberg and W. Kohn, Phys. Rev. **136**, 864 (1964).

[34] W. Kohn and L. J. Sham, Phys. Rev. **140**, 1133 (1965).

[35] R. G. Parr and W. Yang, Density Functional Theory of Atoms and Molecules (Oxford University Press, New York, 1989).

[36] Amsterdam Density Functional Package, release 2001 (Vrije Universiteit, Amsterdam, 2001).

[37] D. Becke, Phys. Rev. A **38**, 3098 (1988).

[38] C. Lee, W. Yang, and G. R. Parr, Phys. Rev. B **37**, 785 (1988).

[39] C. Kittel, Introduction to Solid State Physics, 7th edn. (Wiley, New York, 1996).

Original

Paper

[40] G. Wiesenekker, G. te Velde, and E. J. Baerends, J. Phys. C, Solid State Phys. **21**, 4263 (1988).

[41] R. Hoffmann, Solids and Surfaces: A Chemist's View of Bonding in Extended Structures (VCH, New York, 1988).

[42] G. Landrum and W. Glassey, Yet Another Extended Hückel Molecular Orbital Package (YAeHMOP) (Cornell University, 2001). YAeHMOP is freely available on the www: at http://sourceforge.netprojects/yahemop.

[43] G. Bester and M. Fähnle, Phys. Rev. B **72**, 094102 (2005).

[44] M.-Z. Dang and D. G. Rancourt, Phys. Rev. B **53**, 2291 (1996).

[45] J. F. Valderruten, G. A. Peréz Alcázar, and J. M. Greneche, Rev. Colomb. Fís. **38**, 97 (2006).

[46] A. B. Anderson, J. Am. Chem Soc. **99**, 696 (1977).

[47] W. Moritz, R. Imbihl, R. J. Behm, G. Ertl, and T. Matsushima, J. Chem. Phys. **83**, 1959 (1985).

[48] C. Ashman, S. N. Khanna, and M. R. Pederson, Chem. Phys. Lett. **368**, 257 (2003).

[49] J. V. Badding, R. J. Hemley, and H. K. Mao, Science **253**, 421 (1991).

[50] B. D. Butler and J. B. Chen, Ultramicroscopy **52**, 238 (1993).

[51] D. Tzeli and A. Mavridis, J. Chem. Phys. **116**, 4901 (2002).

[52] Y. Niu, S. Wang, D. Zhao, and C. Wang, J. Phys.: Condens. Matter **13**, 4267 (2001).

[53] R. Wu, A. Freeman, and G. Olson, Phys. Rev. B **53**, 7504 (1996).

[54] R. Fournier, J. Andzelm, A. Goursot, N. Russo, and D. R. Salahub, J. Chem. Phys. **93**, 2919 (1990).

[55] J. H. Onuferko, D. P. Woodruff, and B. W. Holland, Surf. Sci. **87**, 357 (1979).

[56] M. Bader, C. Ocal, B. Millert, J. Haase, and A. M. Bradshaw, Phys. Rev. B **35**, 5900 (1987).

[57] B. D. Butler and J. B. Cohen, Acta Metall. Mater. **41**, 41 (1993).

[58] M. R. Press, S. N. Khanma, P. Jena, and M. J. Puska, Z. Phys. B, Condens. Matter **81**, 281 (1990).

[59] J. A. Slane, C. Wolverton, and R. Gibala, Mater. Sci. Eng. A **370**, 67 (2004).

[60] X. Gong, Z. Zeng, and Q. Zheng, J. Phys.: Condens. Matter **1**, 7577 (1989).

[61] W. Seith, Diffusion in Metallen: Platzwechselreaktionen (Springer, Berlin, 1955).

[62] H. Nakajima and K. Hirano, Trans. Jpn. Inst. Met. **19**, 400 (1978).

[63] J. C. Krause, C. Paudani, and M. I. da Costa, Jr., Hyperfine Interact. **108**, 465 (1997).

[64] V. G. Gavriljuk, V. N. Shivanyuk, and B. D. Shanina, Acta Mater. **53**, 5017 (2005).

[65] A. Juan, L. Moro, G. Brizuela, and E. Pronsato, Int. J. Hydrog. Energy **27**, 333 (2002).

[66] P. Petkov, G. Vayssilov, S. Krüger, and N. Rösch, Chem. Phys. **348**, 61 (2008).

[67] S. Simonetti, L. Moro, E. Gonzalez, G. Brizuela, and A. Juan, Int. J. Hydrog. Energy **29**, 649 (2004).

[68] R. Morrison and N. Boyd, Organic Chemistry (Allyn and Bacon, Boston, MA, 1973).

[69] K. S. Shin, C. G. Park, and M. Meshii, in: Hydrogen Effects in Metals, edited by I. M. Bernstein and A. W. Thompson (TMS-AIME, New York, 1981), pp. 209–218.

[70] E. Pronsato, C. Pistonesi, and A. Juan, J. Phys.: Condens. Matter **16**, 6907 (2004).